

Simulation of high-density water: Its glass transition for various water models

Martin Jehser,¹ Markus Seidl,^{1,2} Clemens Rauer,¹ Thomas Loerting,²
 and Gerhard Zifferer^{1,a)}

¹Department of Physical Chemistry, University of Vienna, Währinger Str. 42, A-1090 Wien, Austria

²Institute of Physical Chemistry, University of Innsbruck, Innrain 52a, A-6020 Innsbruck, Austria

(Received 22 November 2013; accepted 18 March 2014; published online 4 April 2014)

High-density amorphous water is simulated by use of isothermal-isobaric molecular dynamics at a pressure of 0.3 GPa making use of several water models (SPC/E, TIP3P, TIP4P variants, and TIP5P). Heating/cooling cycles are performed in the temperature range 80–280 K and quantities like density, total energy, and mobility are analysed. Raw data as well as the glass transition temperatures T_g observed in our studies depend on the water model used as well as on the treatment of intramolecular bonds and angles. However, a clear-cut evidence for the occurrence of a glass-to-liquid transition is found in all cases. Thus, all models indicate that high-density amorphous ice found experimentally may be a low-temperature proxy of an ultraviscous high-density liquid. © 2014 AIP Publishing LLC. [<http://dx.doi.org/10.1063/1.4869861>]

INTRODUCTION

It is well known that supercooled water forms three amorphous solid states in addition to (at least) 16 crystalline ice phases. These states have been structurally characterized by, e.g., neutron diffraction and may be distinguished, e.g., by their density ρ at 1 bar ranging from $\rho \approx 0.94 \text{ g/cm}^3$ for LDA (low-density amorphous ice) over $\rho \approx 1.13 \text{ g/cm}^3$ for relaxed HDA (high-density amorphous ice) to $\rho \approx 1.26 \text{ g/cm}^3$ in case of VHDA (very high-density amorphous ice).¹ However, there is still controversial discussion if amorphous ices are glasses or nanocrystalline materials.² Contrary to crystalline materials, the former become softer upon heating and transform to a supercooled ultraviscous liquid at the so-called glass transition temperature T_g .³ However, as a matter of fact both the glassy and the liquid state are metastable with respect to the crystalline phase around T_g . Often spontaneous crystallization interferes in experiments aimed at observing and characterizing the metastable liquid. Thus, only the onset of the glass transition region is accessible in experimental studies on water, except in those on confined⁴ and salty water⁵ or hydrated proteins⁶ where crystallization is avoided. Because the ultrahigh heating/cooling rates employed inhibit spontaneous crystallization, molecular dynamics simulations are most valuable for the study of glass transitions and for the investigation of properties of glassy and supercooled water.^{7–11} It has to be noted, though, that the advantage of avoiding crystallization comes with the disadvantage that the huge difference in rates between experiment and simulations hampers attempts of a quantitative comparison. Several methods are suitable to evaluate T_g , all of which are closely related to experimental techniques. First, a kink in the enthalpy $H(T)$ and/or a step-like increase in heat capacity $C_p(T)$ may be used

to locate T_g , in analogy to experiments measuring the calorimetric T_g .^{12,13} Second, sudden changes in molecular mobility can be utilized, which may be determined from mean square displacements of water molecules $msd(T)$ ¹⁴ that are also accessible from neutron scattering experiments. Finally, T_g can be extracted from the location of a kink in the density $\rho(T)$, in analogy to the experimental protocol¹⁵ used for measuring the volumetric T_g .

For HDA, e.g., at a pressure of $p \approx 0.3 \text{ GPa}$ a glass transition was observed in MD simulations with T_g slightly depending on the evaluation method and significantly on the model applied: On average $T_g \approx 189 \text{ K}$ (235 K, 207 K) was obtained for force field COMPASS (SPC/E*, TIP3P*) making use of group based cut-offs,⁹ while lower values $T_g \approx 167 \text{ K}$ (200 K, 178 K) were obtained when treating long range Coulomb interactions by Ewald summation.¹⁰ In addition, in the latter case the density at 80 K was $\approx 0.1 \text{ g cm}^{-3}$ lower compared to truncated Coulomb interactions, and pronounced kinks indicating T_g appeared only in the $H(T)$ but not in the $\rho(T)$ vs. T curves, especially for SPC/E*.

In our earlier work,^{9,10} we have employed force fields with flexible bonds and angles, namely, COMPASS¹⁶ and the TIP3P¹⁷ and SPC/E¹⁸ variants, TIP3P* and SPC/E*, with harmonic bond and angle potentials, $k_l/2 \cdot (l - l_0)^2$ and $k_\theta/2 \cdot (\theta - \theta_0)^2$ taking the unperturbed angle and bond values as well as van der Waals and Coulomb terms from the original models and k_l and k_θ from the CVFF force field.¹⁹

In the present paper, we extend these calculations to the more commonly used original versions TIP3P and SPC/E with fixed bond geometries and to several TIP4P variants. While the former are simple three-point models, the latter are four-point models, in which the positions of the center of mass and the atom charge of oxygen are slightly different. The original set of parameters of TIP4P¹⁷ and of two modifications with fixed bond length and angles, i.e., TIP4P/Ice²⁰ and TIP4P/2005²¹ are applied as well as the flexible water

^{a)} Author to whom correspondence should be addressed. Electronic mail: gerhard.zifferer@univie.ac.at

model TIP4P/2005f²² with a harmonic angle potential and a Morse type bond potential with parameters similar to (but not identical with) TIP4P/2005. Finally, we also use the five-point model TIP5P,²³ where the atom charge of oxygen is symmetrically located at two phantom positions along the lone pair directions. TIP3P* and SPC/E* calculations have been performed by use of the bond and angle parameters implemented in GROMACS²⁴ which are slightly different compared to our former calculations. Test runs, however, revealed that the change in the stiffness of the bond and angle potential left the results unchanged within statistical accuracy.

The general performance of the water models used in this study was tested in a critical survey by Vega and Abascal.²⁵ However, the scoring function in their work did not take into account performance of the models with respect to the properties of amorphous solid states and their glass transition temperatures. For this reason, we here investigate the capability of these models to reproduce the density and glass-to-liquid transition of HDA at 0.3 GPa and compare it with the recent experimental data.

RESULTS AND DISCUSSION

Constant pressure and temperature molecular dynamics simulations (NpT) are performed by use of the open source program GROMACS²⁴ (<http://www.gromacs.org>) applying a leap-frog algorithm for integrating Newton's equations of motion with a time step of 1 fs under control of the Nose-Hoover²⁶ thermostat with an oscillation period of kinetic energy between the system and the reservoir $\tau_t = 0.5$ ps. Isotropic pressure coupling is performed by use of the Parrinello-Rahman²⁷ barostat (pressure time constant $\tau_p = 2.5$ ps). For van der Waals interactions, a cut-off distance of 1.25 nm applying long range dispersion corrections for energy and pressure is used. The same cut-off distance holds true for the real-space part of Coulomb interactions regarding long range terms by use of the PME²⁸ (particle mesh Ewald) summation method.

Boxes with 512, 1024, 2048, or 4096 water molecules (periodic boundary conditions) are prepared at the experimental 1 bar density of HDA to avoid prejudging the results and to allow the system to find its characteristic density upon relaxation. Thus, the initial systems are produced by several nanoseconds NpT relaxation at the target temperature 80 K and pressure 0.3 GPa (3000 bar). Then, the system is heated in steps of 10 K until a maximum temperature (280 K) is reached. Afterwards, a cooling process is initiated by lowering the temperature in steps of 10 K until the lowest temperature (80 K) is reached, and so on. At each temperature, a 50 ps run – corresponding to a heating/cooling rate of 2×10^{11} K/s – is performed using the first half for relaxation and the second for data sampling.

Before presenting a detailed analysis of the T_g behavior let us first look at the structure of models investigated and compare it with experimentally obtained amorphous ice structures. Based on isotope substitution neutron diffraction data (partial) radial distribution functions (RDFs) were derived for a series of amorphous ices.^{1,29-31} The experiment-based oxygen-oxygen RDFs $g_{OO}(r)$ for LDA, HDA, and VHDA

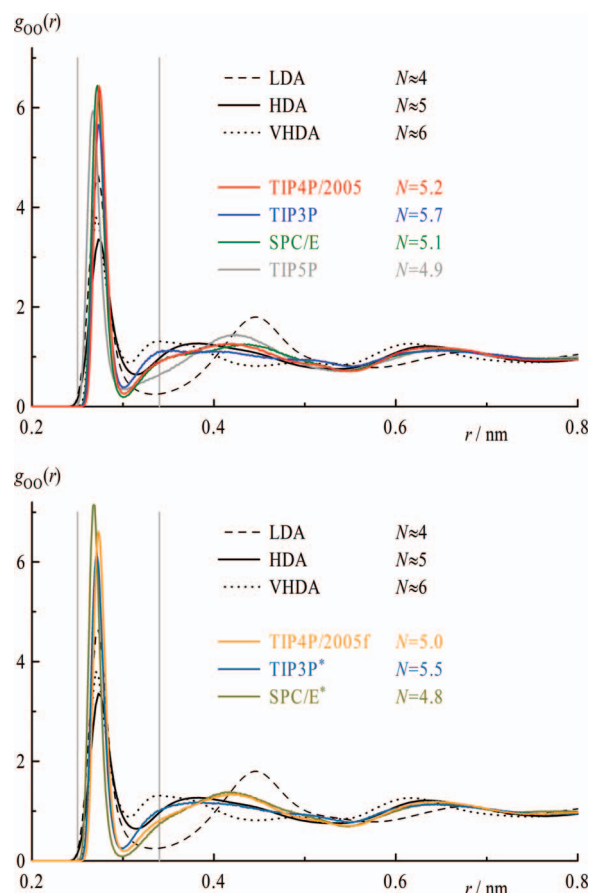


FIG. 1. Partial radial distribution function of the oxygen atoms, $g_{OO}(r)$, for several water models (indicated in the diagrams) at 80 K and 0.3 GPa together with experimental data for LDA (LDA_{II}), HDA (eHDA), and VHDA at 80 K and ambient pressure taken from Ref. 1. N represents first neighbor coordination numbers for oxygen atoms under the respective conditions (within the range 0.25–0.34 nm depicted by vertical lines).

recovered to 80 K and ambient pressure¹ are shown in Figure 1 together with several simulated systems at 80 K and 0.3 GPa. Although the first peak is more pronounced for the simulation data, TIP4P/2005 and TIP4P/2005f most closely resemble the experimental HDA curve. Other TIP4P variants (not shown) coincide fairly well with TIP4P/2005, and SPC/E behaves comparably. On the contrary, the second peak of TIP3P and TIP3P* is shifted toward VHDA while that of TIP5P is much broader.

Real LDA, HDA, and VHDA were found to be fourfold coordinated when considering distances up to 0.31 nm. When considering distances up to 0.34 nm, i.e., not only directly hydrogen-bonded, but also interstitial water molecules, the coordination number remains 4 for LDA and increases to ≈ 5 for HDA and ≈ 6 for VHDA.^{29,30} A comparison of these numbers to the equivalently obtained coordination numbers of the simulated systems (see Table I summarizing the results for all systems evaluated) reveals close similarity with HDA in all cases except for TIP3P and TIP3P* which more closely resemble VHDA at 0.3 GPa.

The quantities calculated in order to obtain T_g values comprise density $\rho(T)$ in g cm^{-3} , enthalpy $H(T)$ in kJ mol^{-1} (calculated from the simulations as the sum of potential energy, kinetic energy, and pV), and in addition the mean square

TABLE I. Summary of characteristic data of the model systems studied ($p = 0.3$ GPa): First neighbor coordination number N for oxygen atoms at 80 K (within the range 0.25–0.34 nm), glass temperatures $T_{g,H}$, $T_{g,msd}$, and $T_{g,\rho}$ obtained via $H(T)$, $msd_{15}(T)$, and $\rho(T)$, as well as the density ρ_g at $T_{g,\rho}$ (heating/cooling rate 2×10^{11} K/s; 3×10^{10} K/s in case of ST2¹¹).

	Water model	N	$T_{g,H}$ (K)	$T_{g,msd}$ (K)	$T_{g,\rho}$ (K)	ρ_g (g cm ⁻³)
Fixed bonds	TIP5P	4.92	205	213	–	–
	TIP4P/2005	5.22	193	199	197	1.142
	TIP4P/Ice	5.17	201	209	193	1.132
	TIP4P	5.15	174	180	215	1.146
	TIP3P	5.67	154	159	176	1.182
	SPC/E	5.11	185	187	221	1.138
	ST2 from Ref. 11	–	212	–	210	1.3
Flexible bonds	TIP4P/2005f	5.03	196	199	203	1.135
	TIP3P*	5.48	175	176	188	1.183
	SPC/E*	4.80	199	215	215	1.138

displacement $msd_{15}(T)$ of oxygen atoms within 15 ps. Comparison of data obtained for different box sizes reveal that apart from a decrease of scattering of $\rho(T)$ data with increasing box size, no significant differences become evident. As an example, details on $\rho(T)$ and $H(T)$ for TIP4P/2005 are shown in Figure 2. Thus, further results for other water models shown in Figures 3 and 4 and T_g values summarized in Table I refer to averages over box sizes of 1024, 2048 and 4096 molecules. Data points of individual models and system sizes are averages over 5 heating/cooling cycles (omitting the first one for relaxation of the system, i.e., for initial equilibration). Standard deviation of T_g data is ≈ 10 –15 K when obtained from density and ≈ 2 –4 K (3–5 K) from enthalpy (msd_{15}).

In Figure 3, different models with fixed bond geometry are compared. The 80 K density is largest for the TIP3P model, followed by TIP4P, TIP4P/2005 (nearly identical to SPC/E), TIP4P/Ice, and TIP5P. With increasing temperature the density decreases, the slope being nearly identical for all

systems below the glass transition temperature $T_{g,\rho}$ which is attained at temperatures 176 K (TIP3P) to 221 K (SPC/E) with TIP4P variants between these limiting values. Above $T_{g,\rho}$ the slope is appreciably larger for TIP3P and almost equal for the other models apart from TIP5P where a specific kink is missing and individual data points are heavily scattering in the range 210–250 K (not shown). Again TIP4P/2005 and SPC/E are rather similar; however, the difference in densities is slightly larger at high temperatures as compared to low ones leading to a larger T_g value for SPC/E. Enthalpies (apart from TIP5P) and mean square displacements are showing the same gradation in the sequence of curves as $\rho(T)$. Contrary to $\rho(T)$ the gradation of T_g values is the same for the two other methods.

In Figure 4, $\rho(T)$ and $H(T)$ traces are compared for fixed and flexible bonds. For all water models, T_g values obtained via $\rho(T)$ and $H(T)$, respectively, are larger in case of flexible bonds and the differences of slopes before and after T_g are

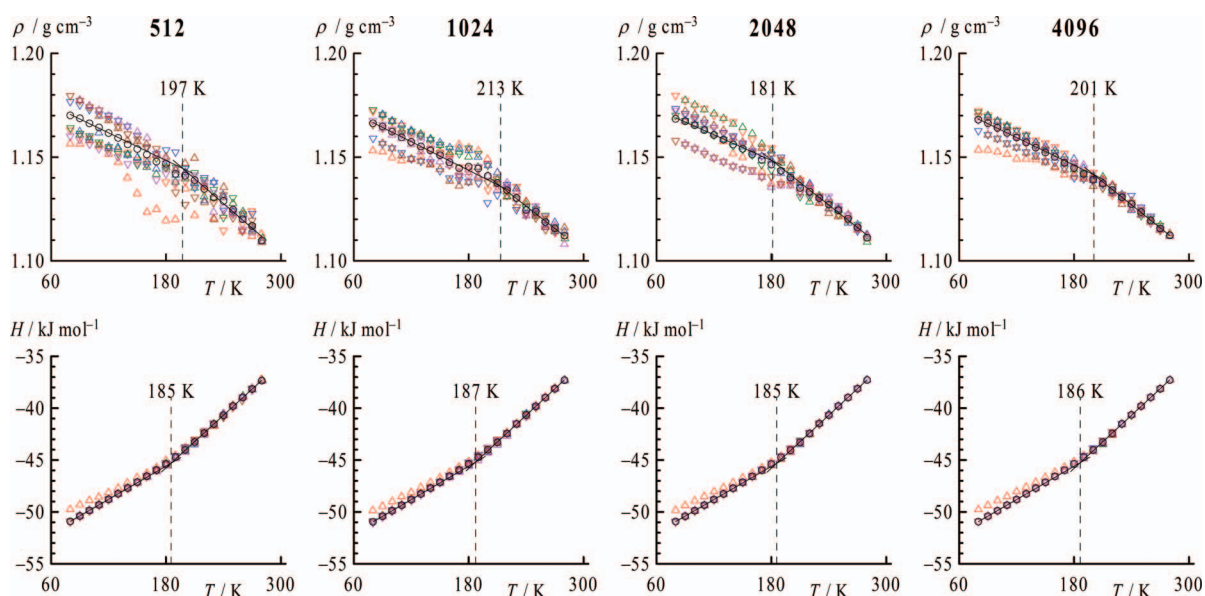


FIG. 2. Density ρ (top) and enthalpy H (bottom) at 0.3 GPa vs. temperature T (heating/cooling rate 2×10^{11} K/s) for TIP4P/2005, as a function of the system size (number of water molecules) indicated in the diagrams. Triangles refer to heating, inverted triangles to cooling runs, and different colors to consecutive cycles (red, green, blue, brown, magenta); circles indicate average values disregarding the first cycle. Vertical lines indicate the glass transition temperature T_g .

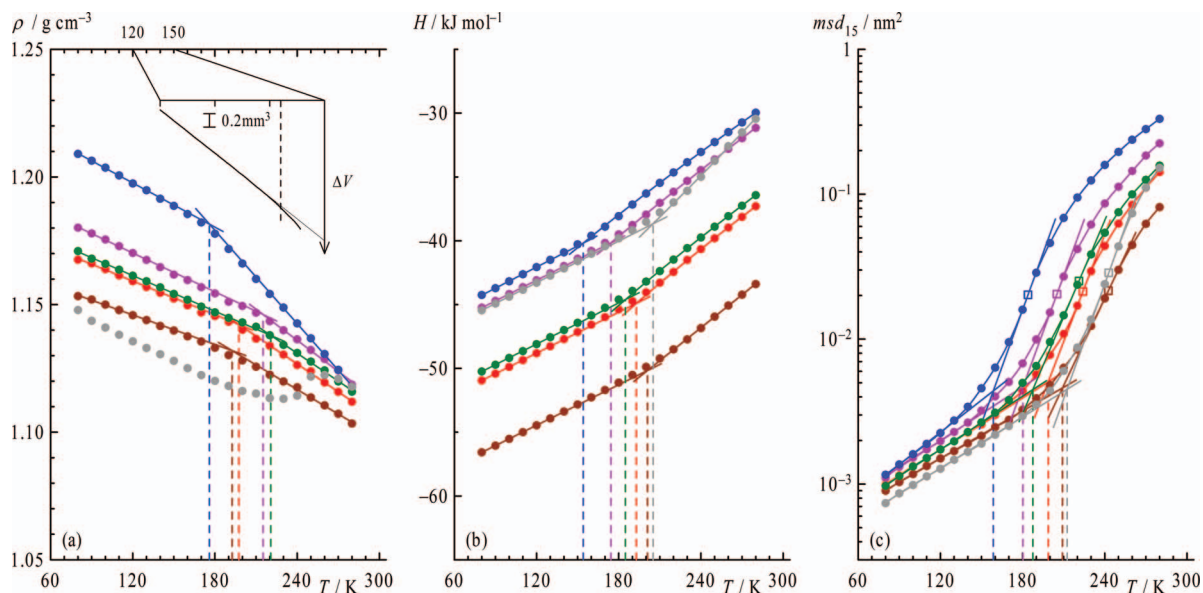


FIG. 3. Density ρ (a), enthalpy H (b), and mobility msd_{15} (c) at 0.3 GPa vs. temperature T (heating/cooling rate 2×10^{11} K/s) for water models TIP3P (blue), TIP4P (magenta), TIP5P (gray), TIP4P/Ice (brown), TIP4P/2005 (red), and SPC/E (green). Squares in the right panel (c) indicate points of inflection. Vertical lines indicate the glass transition temperature T_g . The inset in the left panel (a) shows experimental data¹⁵ (volume change ΔV) for comparison.

more pronounced in case of fixed bond geometry. This result can be rationalized in terms of the degrees of freedom. In the case of flexible bonds, the thermal energy is dissipated over a larger number of motional modes and, thus, the (translational) glass-to-liquid transition is observed at a higher temperature than in the case of fixed bonds.

Recent experimental work using dilatometry indicates that HDA shows a glass transition temperature of 142 ± 2 K at 0.3 GPa.¹⁵ Actually, the volume of HDA increases linearly

with increasing temperature up to ≈ 142 K where a clear-cut deviation from linearity is observed, see inset in Figure 3(a). The onset of this deviation has been identified with T_g .¹⁵

Thus, calculated T_g values are higher by about 40 K compared to the experiment, where the scatter between different models is about 40 K. This is not unexpected because T_g values of simulations quite generally are larger compared to experimental ones. Atomistic molecular dynamics simulations of (cationic) polymethacrylate with varying plasticizer

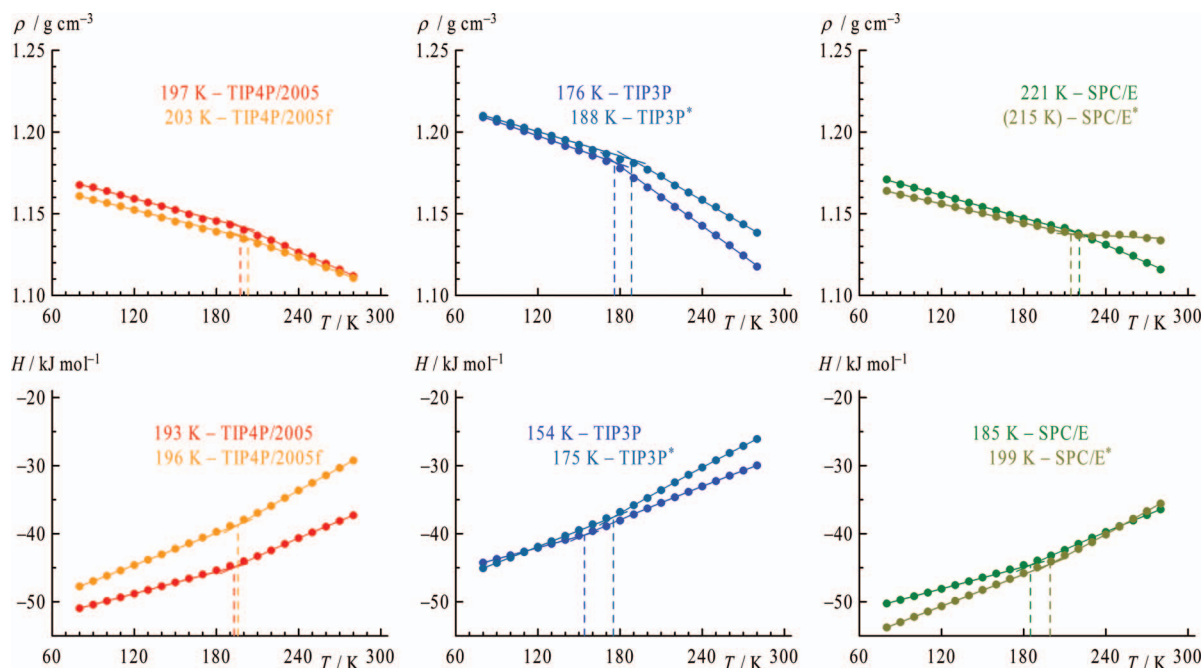


FIG. 4. Density ρ (top) and enthalpy H (bottom) at 0.3 GPa vs. temperature T (heating/cooling rate 2×10^{11} K/s), comparing water models with fixed (TIP4P/2005, TIP3P, SPC/E) and flexible (TIP4P/2005f, TIP3P*, SPC/E*) bonds and angles, respectively. Vertical lines indicate the glass transition temperature T_g .

(triethylcitrate) content, e.g., revealed a linear dependence of the glass transition temperature on the plasticizer content which is (qualitatively) in accordance with DSC experiments, however with lower T_g values in experiments.³² Similarly, predicted values of glass transition temperatures of various amorphous carbohydrates are systematically higher than the experimental ones, but again are showing the same trend as found experimentally and the incremental differences are the same.³³ Thus, trends are obviously correctly predicted by *in silico* experiments with T_g shifted to larger values. The reason for the overestimation is clearly the huge difference in heating rates, which are ultrahigh (2×10^{11} K/s) in the present simulations, but very slow in the volumetric experiments (2 K/min).¹⁵ Actually, when changing the heating/cooling rate by a factor of 10 and comparing simulation runs obtained with 500 ps (“slow”) and 50 ps (“fast”) we found closely related density profiles for both rates; as expected we extracted slightly larger T_g values from the fast 50 ps runs, caused by a tiny shift of densities toward smaller values at low temperatures.¹⁰

Analogous calculations for the TIP4P/2005 system with 50 ps and 500 ps runs (2×10^{11} K/s and 2×10^{10} K/s) revealed the same gradation: Glass temperatures obtained via $H(T)$, $msd_{15}(T)$, and $\rho(T)$ traces – as averages over 4 independent runs with 5 heating/cooling cycles each (2048 H₂O) – read $T_{g,H} = 192.5 \pm 3.5$ K (179.0 ± 1.6 K), $T_{g,msd} = 196.0 \pm 5.0$ K (188.5 ± 3.4 K), and $T_{g,\rho} = 196.7 \pm 10.5$ K (179.5 ± 11.4 K) for 50 ps (500 ps). The former values correspond to the data given in Table I (averages over different systems sizes). The latter show a shift toward smaller transition temperatures with decreasing rate. Further decrease of the rate by a factor 10 (5000 ps runs) yielded $T_{g,H} = 181.0 \pm 4.0$ K, $T_{g,msd} = 186.0 \pm 4.0$ K, and $T_{g,\rho} = 195.0 \pm 15.0$ K; i.e., no significant changes to the 500 ps runs. It should be noted that these latter values result from four independent heating runs only. Thus, a trend toward smaller T_g with decreasing rate could exist, although results at least for the two slower rates are identical within statistical accuracy.

While the influence of the heating rate on T_g has not been investigated experimentally for the case of HDA at 0.3 GPa, a range of calorimetric studies for the case of LDA at 1 bar are available. Here, the calorimetric T_g was found to be 124 K for heating rates of 10 K/h,³⁴ 136 K for heating rates of 30 K/min,³⁵ and 174 K for heating rates of 2.4×10^4 K/s.³⁶ That is, an increase of the heating rate by about seven orders of magnitude increases T_g by 50 K in case of LDA. Assuming a similar increase for HDA at 0.3 GPa the deviations of T_g between slow heating experiments and ultrafast heating simulations noted above are very reasonable.

It should be noted that similar to heating/cooling rates, compression rates in simulations are also rather large as compared to experimental ones. Recently, the influence of compression rates to simulation results of amorphous water has been addressed coming up with the same general features as discussed above.³⁷

Still, it is not straightforward to decide which model most closely resembles real water. However, it may be stated that TIP3P and TIP5P are less suitable for the simulation of HDA. TIP5P simply shows volumetric behavior in contradiction to

all other models and experiment. One reason might be that above T_g the thermal energy is large enough to allow penetration of a fifth molecule into the basic tetrahedral structure (which is most pronounced for TIP5P due to locating the negative charge on the lone pair electrons²⁵) yielding a negative coefficient of thermal expansion above T_g and a density maximum as in case of water at ambient pressure. Actually, simulation runs at 1 bar and 1000 bar show a density maximum for TIP4P/2005 as well. For 2000 and 3000 bar, however, in case of TIP4P/2005 the coefficient of thermal expansion remains positive above T_g while the density maximum is retained for TIP5P.

For TIP3P certainly T_g is closest to the experimental value (not really being indicative due to the discussion on the rate above) but the density is rather large throughout. Experimentally, relaxed HDA (called eHDA) at 80 K and ambient pressure has a density of 1.13 ± 0.01 g cm⁻³.^{1,38} Using the elastic densification upon compression of (unrelaxed) HDA, i.e., ≈ 0.14 g cm⁻³ GPa⁻¹,³⁹ we estimate an experimental density of relaxed HDA at 0.3 GPa and 80 K of 1.17 ± 0.02 g cm⁻³. In fact, only TIP3P clearly does not match the density of real HDA at the given conditions, cf. Figure 3(a). In addition, the first neighbor coordination number in case of TIP3P is significantly larger as expected for HDA, see Table I. Thus, TIP3P more closely simulates VHDA instead of HDA, at least at 0.3 GPa.

Corresponding data for the extensively studied model ST2 (not considered here) may be extracted from Fig. 4 and Fig. 5 of Ref. 11, yielding $T_g \approx 210$ K from density. From the specific heat trace a transition range of ≈ 40 K arises when comparing T_g -onset and T_g -endpoint, in agreement with our data when using different criteria for defining T_g (see Table I). Data for the ST2 model are given in Table I for comparison, identifying $T_{g,H}$ with the inflection point of the specific heat.

CONCLUSIONS

The most important points in summary: (a) Simulation results are independent of the system size apart from larger scattering of densities in case of small boxes. (b) The choice of the model (force field) affects ρ and T_g . (c) For all water models with flexible and fixed bonds, respectively, the glass transition temperature T_g is larger for the former case. (d) Using fixed bond lengths and angles the difference in slopes above and below T_g is more pronounced compared to flexible bonds and angles. (e) The width of HDA’s glass transition for a heating rate of 2×10^{11} K/s can be 40 K (see Table I), which compares to the experimental value of 16 K obtained for a heating rate of 10 K/min (Ref. 13).

Comparing TIP3P, TIP4P variants, and TIP5P several trends are observed: T_g obtained from enthalpy or mobility increase from TIP3P over TIP4P variants to TIP5P. The density at 0.3 GPa and 80 K is largest for TIP3P and smallest for TIP5P. However, in contrast to TIP4P variants, TIP3P does not reproduce the experimental density. In the case of TIP5P, the thermal expansion behavior of HDA in the glass transition region is not appropriately reproduced.

For nearly all properties evaluated ($T_{g,H}$, $T_{g,msd}$, $T_{g,\rho}$, and ρ_g , but not N), data of TIP4P/2005 (similar to SPC/E) are located between results for TIP4P and TIP4P/Ice, with the density at 0.3 GPa and 80 K accurately matching the experimental value of relaxed HDA, i.e., $1.17 \pm 0.02 \text{ g cm}^{-3}$. Thus, the “general purpose model for the condensed phases of water” TIP4P/2005²¹ could also be a good choice for the study of HDA, even though TIP4P/Ice was specifically designed for studies on crystalline and amorphous ices.²⁰

ACKNOWLEDGMENTS

We are grateful to the European Research Council (ERC Starting Grant SULIWA to T.L.), the Austrian Science Fund (FWF START award Y391 to T.L.), and the Austrian Academy of Sciences (DOC fellowship to M.S.) for financial support.

- ¹T. Loerting, K. Winkel, M. Seidl, M. Bauer, C. Mitterdorfer, P. H. Handle, C. G. Salzmann, E. Mayer, J. L. Finney, and D. T. Bowron, *Phys. Chem. Chem. Phys.* **13**, 8783 (2011).
- ²T. Loerting, V. V. Brazhkin, and T. Morishita, *Adv. Chem. Phys.* **143**, 29 (2009).
- ³P. G. Debenedetti, *J. Phys.: Condens. Matter* **15**, R1669 (2003).
- ⁴M. Oguni, Y. Kanke, A. Nagoe, and S. Namba, *J. Phys. Chem. B* **115**, 14023 (2011).
- ⁵C. A. Angell, *Chem. Rev.* **102**, 2627 (2002).
- ⁶G. Sartor, A. Hallbrucker, K. Hofer, and E. Mayer, *J. Phys. Chem.* **96**, 5133 (1992).
- ⁷N. Giovambattista, C. A. Angell, F. Sciortino, and H. E. Stanley, *Phys. Rev. Lett.* **93**, 047801 (2004).
- ⁸I. Brovchenko, A. Geiger, and A. Oleinikova, *J. Chem. Phys.* **123**, 044515 (2005).
- ⁹M. Seidl, T. Loerting, and G. Zifferer, *J. Chem. Phys.* **131**, 114502 (2009).
- ¹⁰M. Seidl, F. Karsai, T. Loerting, and G. Zifferer, *J. Chem. Phys.* **136**, 026101 (2012).
- ¹¹N. Giovambattista, T. Loerting, B. R. Lukanov, and F. W. Starr, *Sci. Rep.* **2**, 390 (2012).
- ¹²O. Andersson, *Proc. Natl. Acad. Sci. U.S.A.* **108**, 11013 (2011).
- ¹³K. Amann-Winkel, C. Gainaru, P. H. Handle, M. Seidl, H. Nelson, R. Böhm, and T. Loerting, *Proc. Natl. Acad. Sci. U.S.A.* **110**, 17720 (2013).
- ¹⁴A. Simperler, A. Kornherr, R. Chopra, W. Jones, W. D. S. Motherwell, and G. Zifferer, *Carbohydr. Res.* **342**, 1470 (2007).
- ¹⁵M. Seidl, M. S. Elsaesser, K. Winkel, G. Zifferer, E. Mayer, and T. Loerting, *Phys. Rev. B* **83**, 100201 (2011).
- ¹⁶D. Rigby, *Fluid Phase Equilib.* **217**, 77 (2004).
- ¹⁷W. L. Jorgensen, J. Chandrasekhar, J. D. Madura, R. W. Impey, and M. L. Klein, *J. Chem. Phys.* **79**, 926 (1983).
- ¹⁸H. J. C. Berendsen, J. R. Grigera, and T. P. Straatsma, *J. Phys. Chem.* **91**, 6269 (1987).
- ¹⁹P. Dauber-Osguthorpe, V. A. Roberts, D. J. Osguthorpe, J. Wolff, M. Genest, and A. T. Hagler, *Proteins: Struct., Funct., Genet.* **4**, 31 (1988).
- ²⁰J. L. F. Abascal, E. Sanz, R. Garcia Fernandez, and C. Vega, *J. Chem. Phys.* **122**, 234511 (2005).
- ²¹J. L. F. Abascal and C. Vega, *J. Chem. Phys.* **123**, 234505 (2005).
- ²²M. A. Gonzalez and J. L. F. Abascal, *J. Chem. Phys.* **135**, 224516 (2011).
- ²³M. W. Mahoney and W. L. Jorgensen, *J. Chem. Phys.* **112**, 8910 (2000).
- ²⁴H. J. C. Berendsen, D. van der Spoel, and R. van Drunen, *Comput. Phys. Commun.* **91**, 43 (1995); E. Lindahl, B. Hess, and D. van der Spoel, *J. Mol. Mod.* **7**, 306 (2001); D. Van Der Spoel, E. Lindahl, B. Hess, G. Groenhof, A. E. Mark, and H. J. C. Berendsen, *J. Comput. Chem.* **26**, 1701 (2005); B. Hess, C. Kutzner, D. van der Spoel, and E. Lindahl, *J. Chem. Theory Comput.* **4**, 435 (2008).
- ²⁵C. Vega and J. L. F. Abascal, *Phys. Chem. Chem. Phys.* **13**, 19663 (2011).
- ²⁶W. G. Hoover, *Phys. Rev. A* **31**, 1695 (1985).
- ²⁷M. Parrinello and A. Rahman, *J. Appl. Phys.* **52**, 7182 (1981).
- ²⁸U. Essmann, L. Perera, M. L. Berkowitz, T. Darden, H. Lee, and L. G. Pedersen, *J. Chem. Phys.* **103**, 8577 (1995).
- ²⁹J. L. Finney, A. Hallbrucker, I. Kohl, A. K. Soper, and D. T. Bowron, *Phys. Rev. Lett.* **88**, 225503 (2002).
- ³⁰D. T. Bowron, J. L. Finney, A. Hallbrucker, I. Kohl, T. Loerting, E. Mayer, and A. K. Soper, *J. Chem. Phys.* **125**, 194502 (2006).
- ³¹K. Winkel, D. T. Bowron, T. Loerting, E. Mayer, and J. L. Finney, *J. Chem. Phys.* **130**, 204502 (2009).
- ³²M. Maus, K. G. Wagner, A. Kornherr, and G. Zifferer, *Mol. Simul.* **34**, 1197 (2008).
- ³³A. Simperler, A. Kornherr, R. Chopra, P. A. Bonnet, W. Jones, W. D. S. Motherwell, and G. Zifferer, *J. Phys. Chem. B* **110**, 19678 (2006).
- ³⁴Y. P. Handa and D. D. Klug, *J. Phys. Chem.* **92**, 3323 (1988).
- ³⁵M. S. Elsaesser, K. Winkel, E. Mayer, and T. Loerting, *Phys. Chem. Chem. Phys.* **12**, 708 (2010).
- ³⁶A. Sepúlveda, E. Leon-Gutierrez, M. Gonzalez-Silveira, C. Rodríguez-Tinoco, M. T. Clavaguera-Mora, and J. Rodríguez-Viejo, *J. Chem. Phys.* **137**, 244506 (2012).
- ³⁷J. Chiu, F. W. Starr, and N. Giovambattista, *J. Chem. Phys.* **139**, 184504 (2013).
- ³⁸T. Loerting, M. Bauer, I. Kohl, K. Watschinger, K. Winkel, and E. Mayer, *J. Phys. Chem. B* **115**, 14167 (2011).
- ³⁹T. Loerting, W. Schustereder, K. Winkel, C. G. Salzmann, I. Kohl, and E. Mayer, *Phys. Rev. Lett.* **96**, 025702 (2006).